



Research Article

Trial to control infectious bursal disease virus using iron oxide chitosan nanocomposite in broiler chickens

Soad A. Nasef¹, Mervat A. Ayoub², Karim M. Selim¹ and Dalia M. A. Elmasry^{3*}

¹ Reference Laboratory of Quality Control of Poultry Production, Animal Health Research Institute, Agricultural Research Center (ARC), Dokki, Egypt

² Pathology Department, Zagazig Province Lab, Animal Health Research Institute, Agricultural Research Center (ARC), Giza, Egypt

³ Nanomaterials Research and Synthesis Unit, Animal Health Research Institute, Agricultural Research Center (ARC), Giza, Egypt



Article History:

Received: 25-Apr-2022

Accepted: 07-Jun-2022

*Corresponding author:

Dalia M. A. Elmasry

dr_daliaelmasry@yahoo.com

Abstract

The present study attempted to control infectious bursal disease virus (IBDV) with iron oxide chitosan nanocomposite as an antiviral compound. The iron oxide chitosan nanocomposite was prepared using the co-precipitation method and characterized by high-resolution transmission electron microscopy (HR-TEM) and cytotoxicity assay on Vero cells. To evaluate the effectiveness of iron oxide chitosan nanocomposite against IBDV, eighty 21-day-old Baladi broiler chicks were divided into four groups (G1-G4). Chicks kept in G1 served as a negative control, while chicks kept in G2 (challenged-non-treated) were challenged orally with IBDV (10^3 EID₅₀/bird). Chicks kept in G3 (challenged-treated) were challenged orally with 10^3 EID₅₀ IBDV/bird and received 1 mL of iron oxide chitosan nanocomposite (1 mg dissolved in 100 mL water) for three days post-inoculation (PI) while chicks kept in G4 (non-challenged-treated) received the same dose of iron oxide chitosan nanocomposite for three successive days. The effectiveness of iron oxide chitosan nanocomposite was assessed based on clinical signs, mortalities, postmortem lesions, and viral RNA load in the bursa of Fabricius samples at the 3rd, 6th, and 9th days PI by isolation onto specific pathogen free embryonated chicken eggs (SPF-ECE) and histopathology. Results revealed that the average particle size of iron oxide chitosan nanocomposite size was found to be 35.1 ± 5 nm. The selected particles exhibited zeta potentials of 16.8 ± 10.9 mV, polydispersity index of 0.91, and iron concentration of 2,625 mg/L. Chicks kept in G2 showed severe clinical signs, including anorexia, ruffled feathers with droopy wings, prostration, and whitish mucoid diarrhea with a mortality rate of 30%. Other groups showed no specific mortalities. The IBDV bursal load was significantly lower ($P < 0.05$) in the challenged-treated chicks ($0.5-1 \log_{10}$) compared to the challenged-non-treated group ($3-6.4 \log_{10}$). Histopathological lesions of the bursa, spleen, thymus, and kidney in the challenged-treated group showed hyperactivity of the lymphoid population compared to necrosis and depletion of lymphoid elements in the challenged control group at the 6th days PI. Based on the current study, iron oxide chitosan nanocomposite showed a promising antiviral activity that could significantly reduce IBDV load in the bursa and decrease pathological changes in lymphoid organs.

Keywords: IBDV, Broiler chicks, Antiviral, Iron oxide chitosan

Citation: Nasef, S. A., Ayoub, M. A., Selim, K. M. and Elmasry, D. M. A. 2022. Trial to control infectious bursal disease virus using iron oxide chitosan nanocomposite in broiler chicken. Ger. J. Vet. Res. 2 (3): 17-27. <https://doi.org/10.51585/gjvr.2022.3.0041>

Introduction

Infectious Bursal Disease (IBD) is a serious disease of chicken causing significant economic losses. The disease causes high mortalities, immunosuppression, and severe lesions in the bursa of Fabricius (Tadesse and Jenbere, 2014; Wahome et al., 2017). IBD is caused by the IBD virus (IBDV), which belongs to the *Avibirnavirus* genus of the *Birnaviridae* family. It is known

that serotype 1 of IBDV is pathogenic to chickens, and the acute course of infection is characterized by diarrhea, prostration, and abrupt mortality in chickens younger than 10 weeks of age. Two serotypes of IBDV serotypes; serotype 1, which is pathogenic to chickens, while serotype 2 is believed to be nonpathogenic.

Based on the antigenic variation and virulence, serotype 1 is divided into several groups (classical

strains, variant strains, and very virulent (vv) strains (Zierenberg et al., 2000). The mortality rates of vvIBDV strains may reach to 60-70% in chickens (Murphy et al., 1999; Abdel-Alim et al., 2003). In Egypt, vv IBDV was reported in 1989; however, the virus still causes significant economic losses despite implementing of intensive vaccination programs (Shehata et al., 2017; Samy et al., 2020; Omar et al., 2021).

Nanotechnology is becoming increasingly important in the diagnosis and management of animal diseases. The use of metal or metal oxide nanoparticles in virus targeting formulations is becoming more common. It promises to improve the agents' diagnostic or therapeutic capabilities while increasing the chances of targeted medication delivery in a novel method. The lowered ratio of viral suspensions after treatment with iron oxide nanoparticles was calculated in a recent study to demonstrate that the iron oxide nanoparticle has antiviral action (Yadavalli and Shukla, 2017). Iron oxide antiviral activity was reported *in-vitro* with more potent suppression at lower doses, possibly due to its small size, simple contact with the virus, and typical spatial organization of the nanoparticles attached (Elechiguerra et al., 2005). Generally, nanoparticles exert their virucidal action through several mechanisms such as i) inhibition of virus-cell receptor binding, ii) reactive oxygen species oxidation, and iii) destructive displacement bonding with critical viral structures (Lin et al., 2021).

Nanoparticles interact with the virus by preferentially binding to the influenza virus protein. Based on the center-to-center distance between nanoparticles, exposed sulfur-bearing residues on protein knobs would be optimal places for engagement with nanoparticles. Because of this interaction, nanoparticles prevent the virus from attaching to host cells (Wieczorek et al., 2020). Although the antiviral function of the composites has yet to be determined the experimental results demonstrated a link between antiviral activity and iron oxide nanoparticle concentrations, suggesting that virions and composites were interacting (Hussain et al., 2006). Additionally, a molecular mechanism of action could result from an interaction of iron oxide with sulfur groups of viral proteins (-SH group protein) in the protein inactivating cell (Mori et al., 2013). However, more clarification is needed on whether and how nanoparticles disrupt membrane function. Consequently, detailed studies of the antiviral mechanism of the iron oxide nanoparticle could lead to the development of functional iron oxide nanoparticles containing materials that would minimize concerns about the risk of the spread of iron oxides nanoparticle to the infection region (Kumar et al., 2019).

Chitosan is a natural polymer derived from alkaline chitin hydrolysis, which occurs in arthropod exoskeletons, crab shells, and insect cuticles. Chitosan and its nanoparticles have attracted considerable attention in the pharmaceutical, food, agricultural, textile, and tissue industries because of their inherent biocompatibility, biodegradability, and lack of toxicity (Dutta et al., 2004). This study aimed to investigate the effect of

iron oxide chitosan nanocomposite on virus load in the bursa of Fabricius and the pathological lesions associated with experimental IBDV infection in susceptible broiler chicks.

Material and methods

Very virulent IBD virus

A very virulent field Egyptian strain of IBDV was obtained from the Reference Laboratory of Veterinary Quality Control on Poultry Production, Egypt. The virus partial VP2 sequence was submitted to the GenBank with accession number OK483322. The strain titer was 10^4 embryonated infective dose 50 (EID₅₀/mL).

Preparation and characterization of iron oxides chitosan nanocomposite

The co-precipitation method was used to prepare the iron oxide chitosan nanocomposite (Rabel et al., 2013). Briefly, 0.55g of ferrous sulfate extra pure, 99.5% (FeSO₄.7H₂O) (SRLPvt. Ltd, Maharashtra, India), and 0.95g of ferric chloride hexahydrate, 98% (FeCl₃.6H₂O) (Himedia, Thane, India), were added to 15 mL double distilled water and stirred for 10 min. The pH was adjusted to 11 by adding an ammonia solution (Merck, Darmstadt, Germany). The black color precipitate of iron oxide nanoparticles was washed several times. After drying, 200 mg chitosan solution (85%) deacetylated (Thermo Fisher GmbH, UK) was added and mixed using a magnetic stirrer for 1 hr until the chitosan-coated iron oxide particles were obtained.

In a high-resolution transmission electron microscopy (HR-TEM), the image JEM 2100F was captured with an accelerating voltage of 200Kv, after dropping benzene solutions of the substances left on the membrane's surface onto copper grids coated with a perforated amorphous carbon film according to Sorour et al. (2021). Fourier Transmittance Infrared FT-IR-6100 Spectrometer measured the bond vibration frequencies in a molecule and was used to determine the functional group. The amount of light absorbed by the sample was measured as wavelength varied. Generally, possess very prominent and characteristic electronic absorptions in the electromagnetic spectrum's near-ultraviolet/visible/near-infrared (UV/VIS/NIR) region. Zeta sizer Nano ZS equipment (Malvern Instruments, Worcestershire, UK) where the diffusion coefficient can be mathematically correlated to the fluctuations of scattered light from particles. The Stokes-Einstein equation was used to calculate the intensity average (Z-average) hydrodynamic diameter from measured diffusivities according to Sorour et al. (2021).

Nano-cytotoxicity of iron oxide chitosan nanocomposite

The African Green Monkey Kidney cells (Vero cells, Nawah, Mokatam, Cairo, Egypt) were cultured in Dulbecco's Modified Eagle Medium (DMEM) (Thermo

Fisher GmbH, UK) containing 100 mg/mL streptomycin, 100 units/mL penicillin, and 10% heat-inactivated fetal bovine serum at 37°C in a humidified 5% (v/v) CO₂ atmosphere. Sulforhodamine B (SRB) assay was used to determine cell viability (Ammerman et al., 2008). Briefly, in 96-well plates, aliquots of 100 mL cell suspension (5×10^3 cells) were incubated in full medium for 24 hrs. Next, another aliquot of 100 mL medium containing iron oxides chitosan nanocomposite at various concentrations ranging from (0.01, 0.1, 1, 10, and 100 µg/mL) was given to the cells. After 72 hrs, cells were fixed by replacing the medium with 150 mL of 10% Trichloroacetic acid (TCA) (Merck, Darmstadt, Germany) and incubated for one hour at 4°C. After removing the TCA solution, cells were washed five times with distilled water. Next, aliquots of 70 mL SRB solution (0.4% w/v) (Merck, Darmstadt, Germany) was added and incubated for 10 min in a dark place at room temperature. Plates were washed three times with 1% acetic acid and air-dried overnight. Then, 150 mL of 10 mM TRIS (Merck, Darmstadt, Germany) was added to dissolve the protein-bound SRB stain. The absorbance was measured at OD₅₄₀ nm using an OIE-compliant BMG LABTECH®-FLUOstar Omega microplate reader (Ammerman et al., 2008). The 50% inhibition concentration (IC₅₀) was then calculated by linear interpolation according to the cell viability results (Wu et al., 2018).

Antiviral activity of iron oxide chitosan nanocomposite *in-vitro*

Vero confluent cells were inoculated with $10^{3.5}$ EID₅₀ IBDV/mL (100 µL) previously treated with (100 µL) iron oxide chitosan (1mg /100 mL) for 30 min. The cytopathic effects (CPEs) and virus titer were evaluated at 5 days post-inoculation and compared with the positive control (IBDV-infected Vero cells) (Khodeir et al., 2016).

***In-vivo* experimental study**

Ethics approval

The Institutional Animal Care and Use Committee (ARC-IACUC) of the Agricultural Research Center have approved the study protocol according to the Animal-Welfare Act of the Ministry of Agriculture in Egypt (approval ARC-AH-19/12).

Experimental design

Eighty 21-day-old in Baladi chicks were divided into four groups (G1-G4) of twenty chicks per group. Feed and water were provided *ad libitum*. Chicks kept in G1 were served as a negative control, while chicks kept in G2 (challenged-non-treated) were challenged orally with IBDV (10^3 EID₅₀/bird). Chicks kept in G3 (challenged-treated) were challenged orally with 1 mL 10^3 EID₅₀ IBDV/bird and received 1 mL iron oxide chitosan nanocomposite (1mg/100 mL) orally for three days post-infection (PI), while chicks kept in G4 (non-challenged-treated) received the same dose of iron oxide chitosan nanocomposite for three successive days as shown in (Table 1). All groups were kept under strict

biosecurity measures. Bursa samples were collected from five birds/group at the 3rd, 6th, and 9th days PI to detect virus load using specific pathogen-free embryonated chicken eggs (SPF-ECE). In addition, tissue samples were collected from the bursa, spleen, thymus, liver, and kidney from experimentally infected and recently dead chicks at 3rd and 6th days PI.

Detection of the iron level in serum

Serum samples were collected from five birds/group for iron level detection in serum. An Iron colorimetric kits (Biodiagnostics, Egypt) was used according to the method described by Dreux (1977), briefly, the serum was deproteinized by trichloroacetic acid and the iron is dissociated from the protein transferrin by hydrochloric acid then reduced to ferrous by thioglycolic acid. The colored complex which the iron forms with bathophenanthroline was measured colorimetrically.

Virus quantification in the bursa of Fabricius

Bursa homogenate was collected from challenged chicks- infected with IBDV in G2 and G3 groups. In addition, virus load was titrated in SPF-ECE obtained from an egg production pathogen-free farm in Cairo, Egypt using the Reed and Muench method (Reed and Muench, 1938).

Pathological examination

The tissue samples collected from all groups at the 3rd and 6th days PI were fixed in 10% neutral buffer formalin solution and then processed using the routine histopathological technique. Paraffin sections of 3-4 micron thickness were prepared and stained with Haematoxylin and Eosin (H&E) stain for examination microscopically (Suvarna et al., 2019). The histopathological lesion grading was calculated by describing the histomorphological changes in five fields per section for each examined organ, according to Gibson-Corley et al. (2013).

Statistical analysis

The data obtained in this study were analyzed using statistical analysis system software (one-way- ANOVA) (SPSS21, 2012). In all cases $p \leq 0.05$ was assumed to indicate significant differences.

Results

Iron oxide chitosan nanocomposite and characterization

Different analytical methods were used to analyze the properties of synthesized iron oxide nanocomposite. The analysis revealed that the concentration of iron oxide in nanocomposite was 2,625 mg/L as determined by the atomic absorption methods. Furthermore, the magnetic nanoparticles bound with chitosan have a well-shaped spherical form with a smooth surface, and the average particle size was around 35.15 nm with a narrow size distribution. As a result, composite nanoparticles are more likely to attract each other to establish a stable state (Figure 1).

The Zeta potential of the synthesized iron oxide chitosan nanocomposite was 16.8 ± 10.9 mV, as a measurement of the conductivity 4.69, viscosity 0.887, and the

Table 1: Mortality rate of experimental groups.

Group	Chicken No.	Challenge ¹	Treatment ²	Mortality ³
G1: Negative control	20	-	-	1/20 (5%)*
G2: Challenged control	20	+	-	6/20(30%) ⁴
G3: Challenged-treated	20	+	+	1/20 (5%)*
G4: Non-challenged-treated	20	-	+	1/20 (5%)*

¹ Challenged with IBDV orally ($10^3\text{EID}_{50}/\text{bird}$).

² Birds received 1ml of iron oxide chitosan nanocomposite (1 mg dissolved in 100 ml water) for three days post-challenge.

³ Asterisks (*) denote non-specific mortalities.

⁴ Mortality between 3-5 days post-challenge.

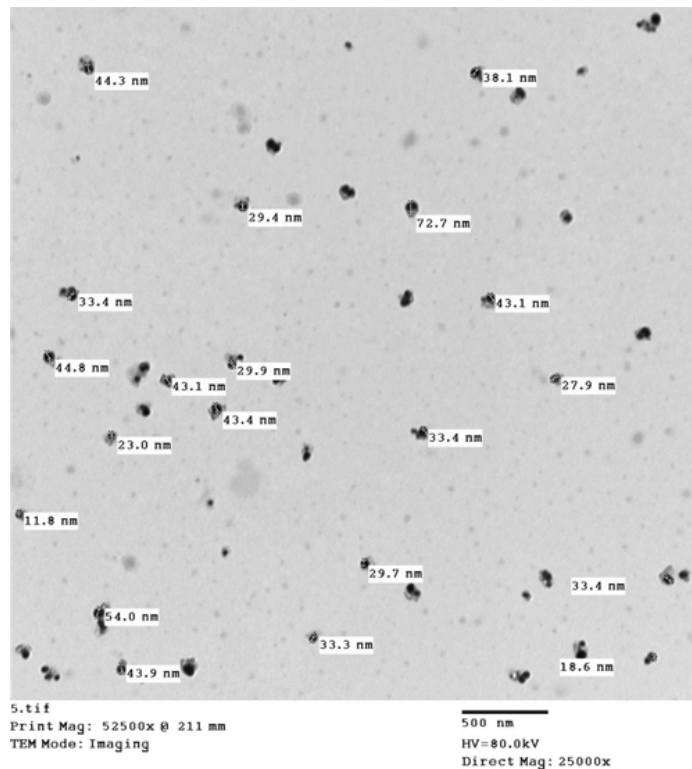


Figure 1: High-resolution transmission electron microscopy (HER-TEM) of magnetic nanoparticles bonded with chitosan with a well-shaped spherical form with a smooth surface, and their average particle size is approximately 35.1 ± 5 nm.

polydispersity indexes (PDI)= 0.91. Compared to pure substances, the FT-IR fingerprint displays the chemical interaction, molecular fingerprint, and detector of functional groups. The highest FT-IR peaks, 3144.75 and 2010.17 cm^{-1} were attributable to phenols and alkynes' O-H and C-H stretch vibrations. Stretching of amino (-NH₂), nitro compounds, alkyl groups, phenols, and carboxylic groups correlate to FT-IR spectral bands at 1752.74, 1630.92, 1402.28, 1113.11, and 841.70 cm^{-1} , respectively. Other brief peaks, ranging from 637.53 to 433.18 cm^{-1} , have been attributed to the presence of Fe oxygen (Figure 2).

Cytotoxicity of iron oxide chitosan nanocomposite

The SRB assay of the synthesized iron oxide chitosan nanocomposite showed that the viability percentage of Vero cells was 95.73% for the high concentration (100 $\mu\text{g}/\text{mL}$) and 98.48% for the low concentration (0.01 $\mu\text{g}/\text{mL}$), indicating that the IC₅₀ is >100 $\mu\text{g}/\text{mL}$ (Figure 3).

Antiviral activity of iron oxide chitosan nanocomposite *in-vitro*

The CPEs of IBDV on Vero cells involved rounding and cell aggregation by 72 hrs PI and became more apparent after five days. In the treated group, the iron oxide chitosan nanocomposite was able to inhibit the IBDV-induced cytopathic effects observed in the IBDV-infected Vero cells (Figure 4).

Experimental study

Clinical signs and gross lesions

Typical clinical signs of IBD were observed in the experimental challenge non-treated group (G2) that was challenged orally with IBDV ($10^3\text{EID}_{50}/\text{bird}$). These observed signs were anorexia, sleepiness, ruffled feathers with droopy wings, prostration, and whitish mucoid diarrhea with a 30% mortality rate. The muscles of the infected chicks showed ecchymotic and paintbrush hemorrhages on the thigh, leg, and pectoral muscles.

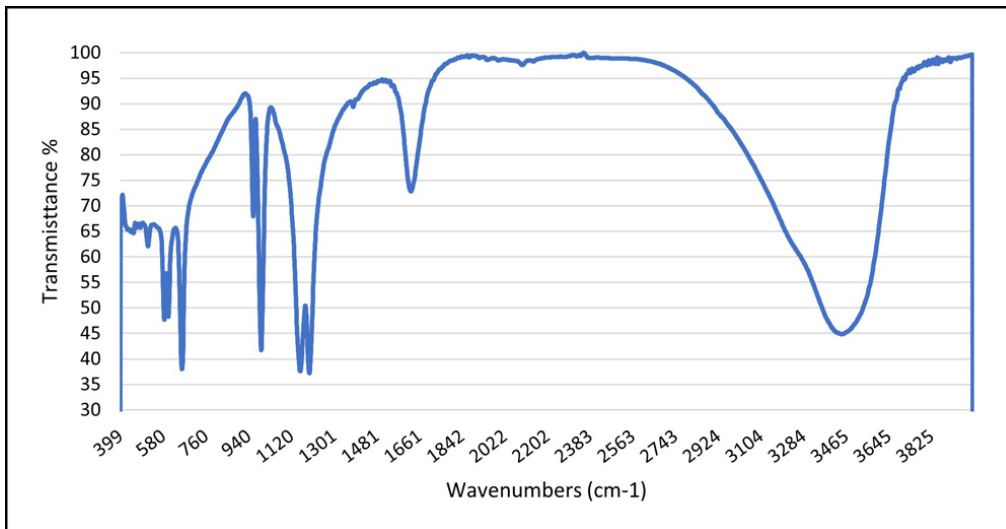


Figure 2: Fourier Transmittance Infrared (FT-IR) spectra of iron oxide chitosan nanocomposite showing specific bands 637.53 to 433.18 cm^{-1} , attributed to the presence of Fe oxygen.

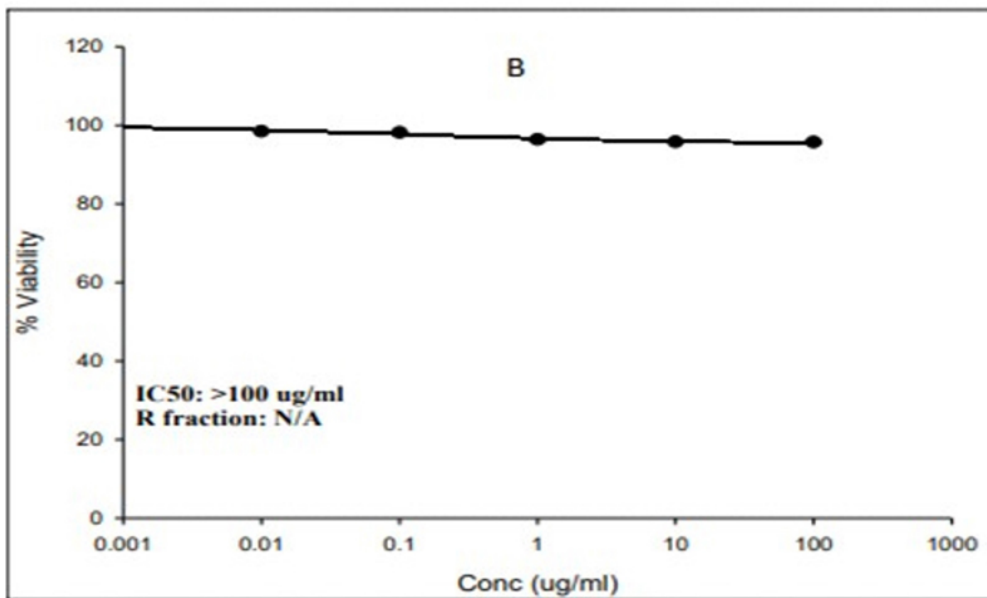


Figure 3: Cell viability % of iron oxide chitosan nanocomposite effect on Vero cells.

The bursae of infected chicks were swollen and hemorrhagic and covered by gelatinous material with yellowish exudate within the lumen on 3rd day PI. On the 6th day PI, the bursa became atrophied. The liver showed peripheral infarction foci, and the kidneys were enlarged and pale. Spleen and thymus were swollen. However, no marked clinical signs or postmortem alteration were observed in all examined organs of other groups and the negative control group (Figure 5).

IBDV load in Bursa of Fabricius

There is no viral detection in the bursa homogenate collected from the negative control birds and birds that received iron oxide chitosan nanocomposite. However, the challenge control group chicks showed viral load with titers of $10^{3-6.4}$ EID₅₀/mL bursal homogenate. On the other hand, the iron oxide chitosan nanocomposite treated group showed significantly lower viral load

titers of $10^{0.5-5}$ EID₅₀/mL bursal homogenate (Table 2).

Detection of iron serum levels

Estimation of iron serum levels showed higher levels in the iron oxide chitosan nanocomposite treated group after being infected with IBDV than in the challenge control group. Meanwhile, the group that received only iron oxide chitosan nanocomposite without virus inoculation showed the highest iron levels ($P < 0.05$), as shown in (Table 3).

Histopathological findings

The bursal lesion scores in the iron oxide chitosan nanocomposite treated group at both 3rd and 6th day PI ranged from none to mild compared to severe lesions in the challenge control group (Table 4). The thymus and kidneys showed very mild lesions represented as congested thymus and blood vessels, and mild degenerative renal epithelium; however, the challenge con-

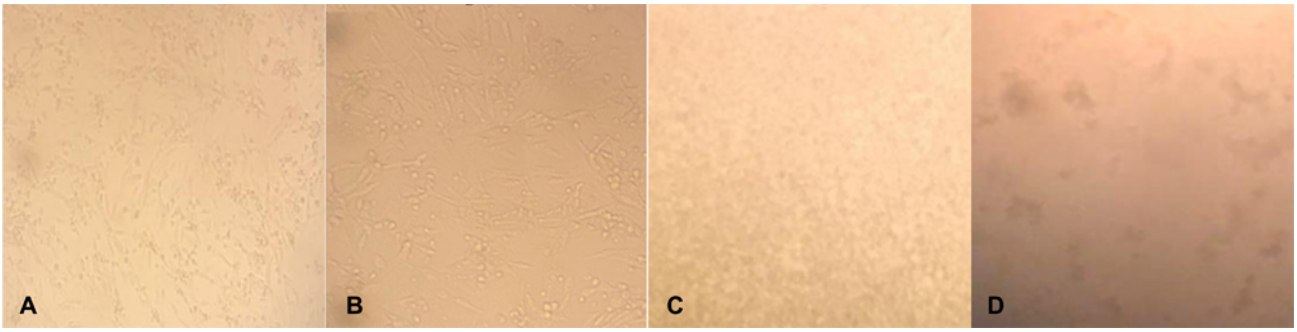


Figure 4: Figure 4. (A) Negative control, (B) Iron oxide chitosan nanocomposite, (C) IBDV and Iron oxide chitosan nanocomposite, and (D) Positive control IBDV infected Vero cells.

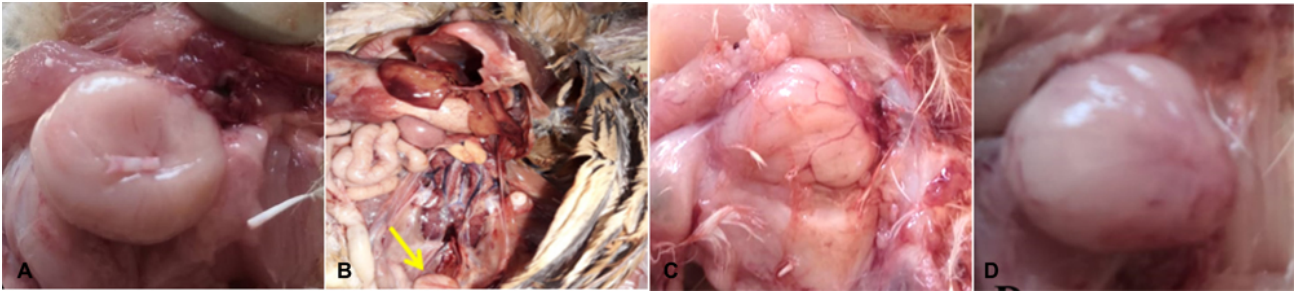


Figure 5: Three-week-old Balady broiler chicks experimentally infected with IBDV. (A) Normal bursa of the control group. (B) Atrophy and hemorrhagic bursa (curved arrow) after six days of infection. (C) Slight enlargement bursa after treatment. (D) Normal bursa of nanocomposite only group.

control group showed severe degenerative renal epithelium, necrotic changes, and renal hemorrhages (Table 4). On the day 6 PI, the liver and spleen lesion scores ranged from mild to moderate lesions in the challenge control group compared to almost normal spleen structure in the treatment group (Table 4).

Histopathological lesions of the bursa and kidney

The challenge control group infected by 10^3EID_{50} IBDV showed central necrosis in bursal follicles and hemorrhages between follicles after three days PI (Figure 6A). At the 6th day PI, atrophied lymphoid populations, and caseous necrosis of most lymphoid follicles center were observed (Figure 6B). The bursae of the iron oxide chitosan treated group showed mild cystic cavitations and heterophil infiltration after three days PI (Figure 6C); however, after six days PI, lymphocytic repopulation of the lymphoid follicles was apparent (Figure 6D). Both non-infected treated and negative control groups showed normal bursal structures.

The positive control group (G2) infected by 10^3EID_{50} IBDV showed focal hemorrhagic areas and severe degeneration and necrosis in some of renal tubules (Figure 6E) and showed degenerative changes in the renal tubular epithelium after six days PI (Figure 6F). Iron oxide chitosan treated group (G3) showed regenerative attempts of the renal tubular epithelium after three days PI (Figure 6G). However, on the 6th day PI showed normal renal tubules (Figure 6H). Non-infected and treated group (G4) showed normal renal tubules and glomerular structures. The kidney lesion score (degenerative renal epithelium, necrotic changes,

and hemorrhages) is shown in Table 4.

Histopathological lesions of spleen and thymus of experimental chicks groups

The positive control group (G2) infected by 10^3EID_{50} IBDV showed necrosis in most lymphoid follicles and the per-arterial lymphoid sheaths and significant lymphocytic depletion of the lymphoid follicles after three days of infection (Figure 7A). However, after six days of infection, it showed edema and necrotic cells of the red pulp (Figure 7B). Iron oxide chitosan treated group (G3) showed congestion of blood vessels after three days PI (Figure 7C). Furthermore, the treated group (G3) showed repopulation of lymphocytes of the lymphoid follicles after six days PI (Figure 7D). Non-infected and treated group (G4) with iron oxide chitosan showed normal white and red pulp.

The positive control group (G2) infected by 10^3EID_{50} IBDV revealed necrosis of most lymphoid lobules, hemorrhages throughout parenchyma, and marked congestion in blood vessels after three days of infection (Figure 7E), and a reduction in lymphoid populations after six days of infection (Figure 7F). Iron oxide chitosan treated group (G3) revealed moderate activity of cortical and medullary lymphoid contents of thymic nodules and dilated septal blood vessels at three days PI (Figure 7G). Moreover, after six days PI showed congestion of blood vessels, apparently normal cortical and medullary lymphoid population (Figure 7H). Non-infected and treated group (G4) with iron oxide chitosan showed normal lymphatic structures. The thymus lesion score (necrotic lymphocytes, Hemorrhages, and congestion) is shown in Table 4.

Table 2: IBDV load in bursal homogenate at 3, 6, and 9 days post infection (DPI).

Group ¹	Virus titers (log ₁₀ EID ₅₀ /mL)		
	3 DPI	6 DPI	9 DPI
G1: Negative control	0.0	0.0	0.0
G2: Challenged control	3.0	4.5	6.4
G3: Challenged-treated	1.4	0.5	0.0
G4: Non-challenged-treated	0.0	0.0	0.0

¹ Challenged with IBDV orally (10³EID₅₀/bird). Treated birds received 1 mL of iron oxide chitosan nanocomposite (1 mg dissolved in 100 mL water) for three days post infection.

Table 3: Iron serum levels at 3, 6, and 9 days post infection (DPI).

Group ¹	Iron serum level (μg/dl) ²		
	3 DPI	6 DPI	9 DPI
G1: Negative control	102.66±8.03 ^{ab}	109.66±7.9 ^{ab}	111.67±10.41 ^a
G2: Challenged control	68.33±5.68 ^c	58.67±4.16 ^c	45.09±13.74 ^b
G3: Challenged-treated	93±6.08 ^b	101.33±3.06 ^b	105.05±5.01 ^a
G4: Non-challenged-treated	111.6±2.89 ^a	117.3±2.52 ^a	137.76±28.11 ^a

¹ Challenged with IBDV orally (10³EID₅₀/bird). Treated birds received 1 mL of iron oxide chitosan nanocomposite (1 mg dissolved in 100 mL water) for three days post-challenge. Groups followed by different superscript small letters indicate significant differences (p<0.05).

Table 4: Summarized histopathological lesion scores in different experimental groups at 3 and 6 days post infection (DPI).

Organ	Lesions	G2: Challenge control ¹		G3: Challenged-treated ²		G4: Non-challenged treated ³
		3 DPI	6 DPI	3 DPI	6 DPI	
Bursa	Necrotic lymphoid follicles	++ ⁴	++	+	-	-
	Atrophied lymphoid populations	+	++	+	+	-
	Hemorrhages	+++	+	-	-	-
	Heterophilic infiltration	++	+	+	-	-
Spleen	Necrotic lymphoid follicles	++	+	-	-	-
	Edema	+	+	-	-	-
	Congested blood vessels	+	++	+	-	-
Thymus	Necrotic lymphocytes	++	++	-	-	-
	Congestion ++	+	+	+	-	-
	Hemorrhages +	+	-	-	-	-
Liver	Necrotic areas	++	+	-	-	-
	Inflammatory cells infiltrations	+++	++	+	+	-
	Congested blood vessels	++	+	+	-	-
Kidney	Degenerative renal epithelium	+++	++	+	-	-
	Necrotic changes	++	+	-	-	-
	Hemorrhages	++	+	-	-	-

¹ Challenged with IBDV orally (10³EID₅₀/bird).

² Birds were challenged with IBDV orally (10³EID₅₀/bird) then received 1 mL of iron oxide chitosan nanocomposite (1 mg dissolved in 100 mL water) for three days post-challenge.

³ Birds received 1 mL of iron oxide chitosan nanocomposite (1 mg dissolved in 100 mL water) for three days post-challenge.

⁴ Abbreviations: -,+,++,and +++ represent none, mild, moderate and severe tissue alterations respectively.

Discussion

The current study provides new insights into the significance of iron oxide chitosan nanocomposite as a potent inhibitor of the IBD virus and rationalizes its development. Previous studies found that iron oxide nanoparticles' optical and structural properties exhibit remarkable changes when coated with organic polymers. Due to the presence of -NH₂ groups on the surface of the FeO nanoparticle after adding chitosan, the

surface charge substantially changed to positive values +12.9 mV. Hence, chitosan-coated magnetic nanoparticles are non-cytotoxic and highly biocompatible at typical concentrations. Metal-oxygen (Fe=O) bonds were detected in the FT-IR spectrum at 500–800 cm⁻¹, while amino groups (-NH₂) were detected at 1,646 cm⁻¹, confirming the presence of chitosan in the produced chitosan-FeO nanocomposite (Pham et al., 2016; Bharathi et al., 2019a,b).

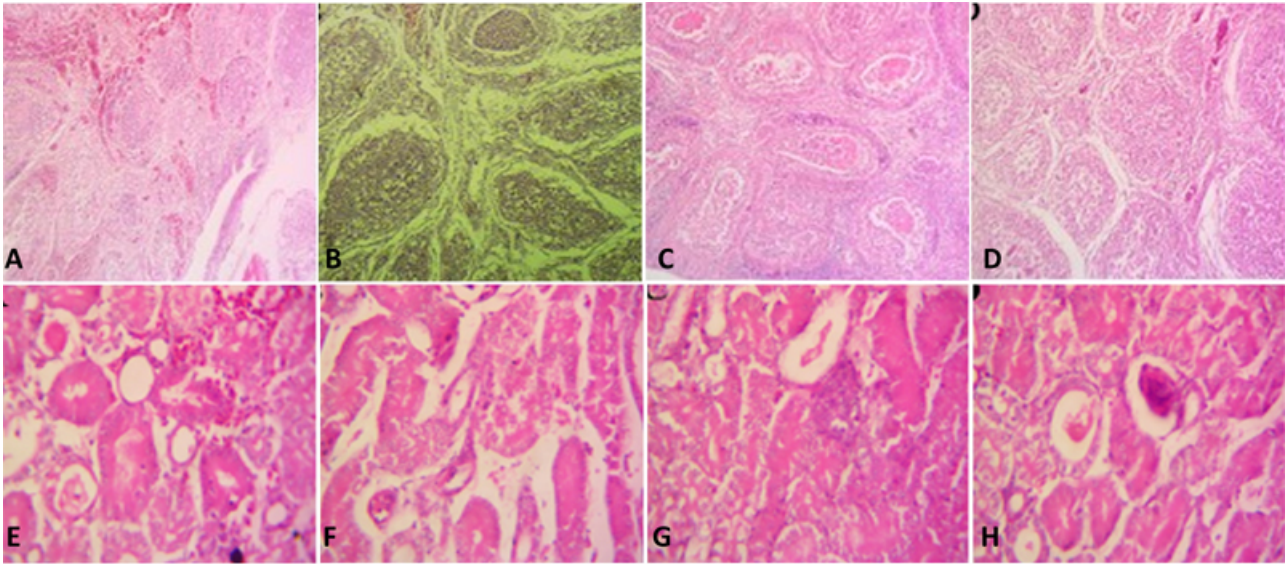


Figure 6: Histopathological lesions of the bursa and kidney of experimental groups. (A) The bursa of challenge control at three days PI showed cystic cavitation, necrosis of most bursal follicles, and hemorrhages between the follicles. (B) The bursa of challenge control at six days PI showed atrophied lymphoid populations and caseous necrosis of most lymphoid follicles center. (C) The bursa of the infected and treated group at three days PI showed mild cystic cavitation and heterophil infiltration. (D) The bursa of the infected and treated group at six days PI showed lymphocytic repopulation of the lymphoid follicles. (E) Challenge control group at three days PI showing focal hemorrhagic area and severe degeneration and necrosis of some renal tubules. (F) Challenge control group at six days PI showing degenerative changes of renal tubular epithelium. (G) The infected and treated group at three days PI showed regenerative attempts of renal tubular epithelium. (H) The infected and treated group at six days PI showed normal renal tubules. H&E $\times 400$.

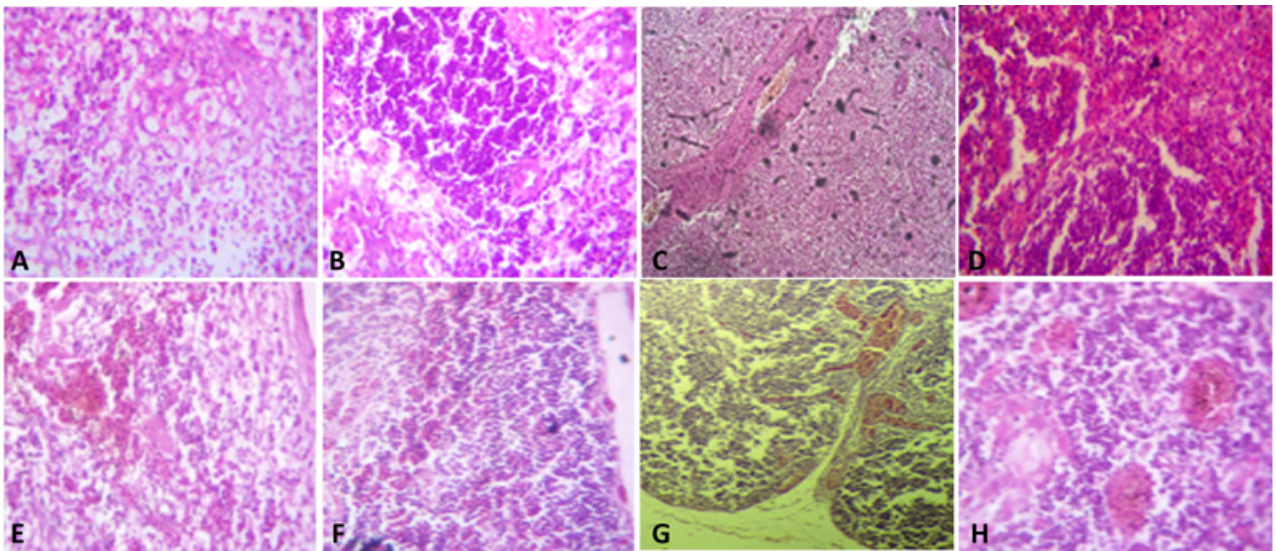


Figure 7: Histopathological lesions of spleen and thymus of experimental chick groups. (A) Challenge the control group at three days PI, the spleen showing necrosis of most lymphoid follicles. (B) Challenge control group at six days PI the spleen showing edema and necrotic cells of the red pulp (C) Infected and treated group at three days PI showing congestion of blood vessels. (D) Infected and treated group at six days PI showing repopulation of lymphocytes of the lymphoid follicles. (E) Thymus in the challenge control group at three days PI showing necrosis of most lymphoid lobules, marked congestion of blood vessels, and hemorrhages throughout the parenchyma. (F) Challenge control group at six days PI showing reduced lymphoid populations. (G) Infected and treated group at three days PI showing moderate activity of cortical and medullary lymphoid contents of thymic nodules and dilated septal blood vessels. (H) Infected and treated group at six days PI showing mild congestion of blood vessels, normal cortical and medullary lymphoid population, and normal Hassall's corpuscles. H&E $\times 400$.

Testing of Fe₃O₄ against the pandemic H1N influenza virus with the 10 to 15 nm iron oxide nanoparticles (IO-NPs) demonstrated that they could bind to the virus and prevent the virus adsorption (Kumar et al., 2019). Also, a molecular docking study of IO-NPs (Fe₂O₃ and Fe₃O₄) with the spike (S) protein receptor-binding domain (S1-RBD) of the Severe Acute Respiratory Syndrome– Coronavirus 2 (SARS-CoV2) led to the interaction of Fe₃O₄ with S1-RBD involved the formation of four hydrogen bonds. Furthermore, the hydrophobic interactions of the tested iron oxide nanoparticles with Leu455, Ser494, and Phe497 in the active site of S1-RBD were found to prevent the SARS-CoV2 virus adsorption to host cells (Abo-Zeid et al., 2020). The microbicidal potential of (NPs) is thought to be a size-dependent activity, with the smaller the size, the higher the potential. This could be due to "spatial binding restriction" between NPs and viral particles (Elechiguerra et al., 2005). Complex antiviral nanoparticles were found to have minimal or low cytotoxicity *in-vivo* (Lysenko et al., 2018).

Results showed that nanocomposite decreased the IBDV replication. Furthermore, the IBDV titers were reduced after 3-9 days PI when exposed to the nanocomposite. Specific receptors important in the IBDV component and entry into the host cells are not occupied (Zhu et al., 2008); therefore, the test findings suggest that the nanocomposite may interfere with several IBDV life cycle stages following viral adsorption and internal cell internalization. Although the mechanism of the composites as antiviral has yet to be found, experimental evidence showing a link between antiviral activity and iron oxide nanocomposite concentrations suggests that the virions and composites interacted. Interaction of iron oxide with sulfur groups of viral proteins in the cell could be the molecular process that is inactivating the proteins (Mori et al., 2013).

During the first 24 hrs of virus infection, the antiviral activity of iron oxide nanoparticles, as detected by viral RNA transcripts changes using RT-PCR, revealed a reduction in the IBDV transcripts (80 fold). Moreover, no marked clinical signs were noticed, and no mortalities were recorded in the nanocomposite treated group. These findings open a new approach for using of IP-NPs as an antiviral agent (Kumar et al., 2019).

Initial swelling of the primary and secondary lymphoid organs of chicks, significant hemorrhages, and acute inflammation characterized by hyperemia followed by severe atrophy of the primary lymphoid organs are the predominant gross abnormalities during the acute phase of IBDV (Sá e Silva et al., 2016). In this investigation, the field virus was found to have the ability to cause severe gross lesions in the bursa, thymus, and spleen. On day 6 PI, the principal lymphoid organs began to atrophy rapidly and noticeably. Lesions in the thymus, bursa, and spleen of IBDV infected chicks showed severe clinical disease correlated with peak mortality and gross lesions at the acute phase of the disease, resulting in diminished immune-protective efficacies (Aliyu et al., 2016).

In the current investigation, significant depletion of

lymphoid cells, reticular cell hyperplasia, edema, hemorrhages, congestion of blood vessels, atrophy, and fibroplasia were seen, followed by hyperplasia of reticular cells in the bursa, thymus, and spleen. On the 6th day PI, complete damage to the bursa, including marked desquamation of epithelial lining and failure of the bursa to repopulate with lymphocytes, caused premature regression of the bursa in the chicks that survived, which could affect B-cell function, reduce immune function, and damage the bursa. This could explain why chicks suffer from immunosuppression when they have IBD (Eterradossi and Saif, 2013).

Pathological and histopathological observations showed that the iron oxide chitosan nanocomposite ameliorated both gross and histopathological lesions. The exposed sulfur-bearing residues of the protein knobs would be attractive sites for nanoparticle interaction. Moreover, the regular spatial arrangement of the attached nanoparticles, the center-to-center distance between nanoparticles, and the fact that the exposed sulfur-bearing residues of the protein knobs would be attractive sites for nanoparticle interaction suggest that nanoparticles interact with the virus via preferential binding to the protein knobs of infectious disease virus. The decreased ratio of viral suspensions after treatment with iron oxide NPs was used to determine the antiviral activity of the iron oxide NPs. Nanoparticles prevent the virus from binding to host cells as a result of this interaction, as demonstrated *in-vitro* (Elechiguerra et al., 2005).

Conclusion

Our results provide new insights into the importance of iron oxide chitosan nanocomposite as a potent inhibitor of the IBDV and rationalize its development. We assume that the method discussed here can develop medically appropriate viricidal drugs to suppress viral infections. It should be emphasized that the proposed approach is fundamentally broad in nature, allowing for the possible prevention and treatment of multiple viral infections with a single medication, a significant benefit, mainly in virology, where rapid and often sudden infections occur.

Attempted treatment for control of IBD by the antiviral iron oxide chitosan nanocomposite administered orally could significantly reduce virus load in the bursa and ameliorate the clinical and pathological lesions induced by IBDV. However, future investigations are needed to evaluate the role of iron oxide chitosan nanocomposite as a preventive antiviral drug under field and laboratory conditions.

Article Information

Funding. This research received no funds.

Conflict of Interest. The authors have no conflict of interest to declare.

References

- Abdel-Alim, G., Awaad, M.H.H., Saif, Y.M., 2003. Characterization of Egyptian field strains of infectious bursal disease virus. *Avian Diseases* 47, 1452–1457. [10.1637/7032](https://doi.org/10.1637/7032).
- Abo-Zeid, Y., Ismail, N.S.M., McLean, G.R., Hamdy, N.M., 2020. A molecular docking study repurposes FDA approved iron oxide nanoparticles to treat and control COVID-19 infection. *European Journal of Pharmaceutical Sciences* 153, 105465. [10.1016/j.ejps.2020.105465](https://doi.org/10.1016/j.ejps.2020.105465).
- Aliyu, H.B., Sa'idu, L., Jamilu, A., Andamin, A.D., Akpavie, S.O., 2016. Outbreaks of virulent infectious bursal disease in flocks of battery cage brooding system of commercial chickens. *Journal of Veterinary Medicine* 2016, 8182160. [10.1155/2016/8182160](https://doi.org/10.1155/2016/8182160).
- Ammerman, N.C., Beier-Sexton, M., Azad, A.F., 2008. Growth and maintenance of Vero cell lines. *Current Protocols in Microbiology* Appendix 4, Appendix 4E. [10.1002/9780471729259.mca04es11](https://doi.org/10.1002/9780471729259.mca04es11).
- Bharathi, D., Ranjithkumar, R., Chandarshekar, B., Bhuvaneshwari, V., 2019a. Preparation of chitosan coated zinc oxide nanocomposite for enhanced antibacterial and photocatalytic activity: As a bionanocomposite. *International Journal of Biological Macromolecules* 129, 989–996. [10.1016/j.ijbiomac.2019.02.061](https://doi.org/10.1016/j.ijbiomac.2019.02.061).
- Bharathi, D., Ranjithkumar, R., Vasantharaj, S., Chandarshekar, B., Bhuvaneshwari, V., 2019b. Synthesis and characterization of chitosan/iron oxide nanocomposite for biomedical applications. *International Journal of Biological Macromolecules* 132, 880–887. [10.1016/j.ijbiomac.2019.03.233](https://doi.org/10.1016/j.ijbiomac.2019.03.233).
- Dreux, C., 1977. Selected method. Analysis of human serum: assay of iron II. Method using bathophenanthroline Se-Iron II (bathophenanthroline). *Annales de Biologie Clinique* 35, 275–277. URL: <https://www.ncbi.nlm.nih.gov/pubmed/900604>.
- Dutta, P., Dutta, J., Tripathi, V., 2004. Chitin and chitosan: Chemistry, properties and applications. *Journal of Scientific and Industrial Research* 63, 20–31.
- Elechiguerra, J.L., Burt, J.L., Morones, J.R., Camacho-Bragado, A., Gao, X., Lara, H.H., Yacaman, M.J., 2005. Interaction of silver nanoparticles with HIV-1. *Journal of Nanobiotechnology* 3, 6. [10.1186/1477-3155-3-6](https://doi.org/10.1186/1477-3155-3-6).
- Eterradossi, N., Saif, Y., 2013. Infectious bursal disease, in: Swayne, D.E. (Ed.), *Diseases of Poultry*. Wiley, pp. 219–246. URL: <https://onlinelibrary.wiley.com/doi/10.1002/9781119421481.ch7>, [10.1002/9781119421481.ch7](https://doi.org/10.1002/9781119421481.ch7).
- Gibson-Corley, K.N., Olivier, A.K., Meyerholz, D.K., 2013. Principles for valid histopathologic scoring in research. *Veterinary Pathology* 50, 1007–1015. [10.1177/0300985813485099](https://doi.org/10.1177/0300985813485099).
- Hussain, S.M., Javorina, A.K., Schrand, A.M., Duhart, H.M., Ali, S.F., Schlager, J.J., 2006. The interaction of manganese nanoparticles with PC-12 cells induces dopamine depletion. *Toxicological Sciences* 92, 456–463. [10.1093/toxsci/kf1020](https://doi.org/10.1093/toxsci/kf1020).
- Khodeir, M., El Tarabeily, M., El Masry, H., Abdelwahab, S., Fawzy, M., 2016. Comparative studies on infectious bursal disease virus propagated in chicken eggs and vero cell culture. *Suez Canal Veterinary Medicine Journal* 21, 109–120. [10.21608/scvmj.2016.62766](https://doi.org/10.21608/scvmj.2016.62766).
- Kumar, R., Nayak, M., Sahoo, G.C., Pandey, K., Sarkar, M.C., Ansari, Y., Das, V.N.R., Topno, R.K., Bhawna, Madhukar, M., Das, P., 2019. Iron oxide nanoparticles based antiviral activity of H1N1 influenza a virus. *Journal of Infection and Chemotherapy* 25, 325–329. [10.1016/j.jiac.2018.12.006](https://doi.org/10.1016/j.jiac.2018.12.006).
- Lin, N., Verma, D., Saini, N., Arbi, R., Munir, M., Jovic, M., Turak, A., 2021. Antiviral nanoparticles for sanitizing surfaces: A roadmap to self-sterilizing against COVID-19. *Nano Today* 40, 101267. [10.1016/j.nantod.2021.101267](https://doi.org/10.1016/j.nantod.2021.101267).
- Lysenko, V., Lozovski, V., Lokshyn, M., Gomeniuk, Y.V., Dorovskih, A., Rusinchuk, N., Pankivska, Y., Povnitsa, O., Zagorodnya, S., Tertykh, V., Bolbukh, Y., 2018. Nanoparticles as antiviral agents against adenoviruses. *Advances in Natural Sciences* 9, 025021. [10.1088/2043-6254/aac42a](https://doi.org/10.1088/2043-6254/aac42a).
- Mori, Y., Ono, T., Miyahira, Y., Nguyen, V.Q., Matsui, T., Ishihara, M., 2013. Antiviral activity of silver nanoparticle/chitosan composites against H1N1 influenza a virus. *Nanoscale research letters* 8, 93. [10.1186/1556-276X-8-93](https://doi.org/10.1186/1556-276X-8-93).
- Murphy, F.A., Gibbs, E.P.J., Horzinek, M.C., Studdert, M.J., 1999. *Birnaviridae*, in: Murphy, F. (Ed.), *Veterinary Virology*. Elsevier, p. 629.
- Omar, S.E., Moneim, W.A., Abdelhalim, A., Yehia, N., 2021. Genetic evolution of infectious bursal disease virus isolated from chicken poultry flocks in Egypt. *Journal of World's Poultry Research* 11, 215–222. [10.36380/jwpr.2021.26](https://doi.org/10.36380/jwpr.2021.26).
- Pham, X.N., Nguyen, T.P., Pham, T.N., Tran, T.T.N., Tran, T.V.T., 2016. Synthesis and characterization of chitosan-coated magnetite nanoparticles and their application in curcumin drug delivery. *Advances in Natural Sciences: Nanoscience and Nanotechnology* 7, 045010. [10.1088/2043-6262/7/4/045010](https://doi.org/10.1088/2043-6262/7/4/045010).
- Rabel, A.M., Jayanthi, V., Raj, N.N., Ramachandran, D., Brjitta, J., 2013. Synthesis and characterization of chitosan-coated iron oxide nanoparticles, in: *International Conference on Advanced Nanomaterials & Emerging Engineering Technologies*, IEEE, pp. 569–571. [10.1109/ICANMEET.2013.6609367](https://doi.org/10.1109/ICANMEET.2013.6609367).
- Reed, L., Muench, H., 1938. A simple method of estimating fifty per cent endpoints. *American Journal of Epidemiology* 27, 493–497. [10.1093/oxfordjournals.aje.a118408](https://doi.org/10.1093/oxfordjournals.aje.a118408).
- Samy, A., Courtillon, C., Briand, F.X., Khalifa, M., Selim, A., Arafa, A.E.S., Hegazy, A., Eterradossi, N., Soubies, S.M., 2020. Continuous circulation of an antigenically modified very virulent infectious bursal disease virus for fifteen years in Egypt. *Infection, Genetics and Evolution* 78, 104099. [10.1016/j.meegid.2019.104099](https://doi.org/10.1016/j.meegid.2019.104099).
- Shehata, A.A., Sultan, H., Halami, M.Y., Talaat, S., Vahlenkamp, T.W., 2017. Molecular characterization of very virulent infectious bursal disease virus strains circulating in egypt from 2003 to 2014. *Archives of Virology* 162, 3803–3815. [10.1007/s00705-017-3554-3](https://doi.org/10.1007/s00705-017-3554-3).
- Sá e Silva, M., Rissi, D.R., Swayne, D.E., 2016. Very virulent infectious bursal disease virus produces more-severe disease and lesions in specific-pathogen-free (SPF) leghorns than in SPF broiler chickens. *Avian Diseases* 60, 63–66. [10.1637/11230-070615-ResNote.1](https://doi.org/10.1637/11230-070615-ResNote.1).
- Sorour, H.K., Hosny, R.A., Elmasry, D.M.A., 2021. Effect of peppermint oil and its microemulsion on necrotic enteritis in broiler chickens. *Veterinary World* 14, 483–491. [10.14202/vetworld.2021.483-491](https://doi.org/10.14202/vetworld.2021.483-491).
- Suvarna, S.K., Layton, C., Bancroft, J.D. (Eds.), 2019. *Bancroft's theory and practice of histological techniques*. Elsevier. [10.1016/C2015-0-00143-5](https://doi.org/10.1016/C2015-0-00143-5).

- Tadesse, B., Jenbere, S., 2014. Sero-prevalence of infectious bursal disease in backyard chickens at selected woredas of Eastern Ethiopia. *Journal of Biology, Agriculture and Healthcare* 4, 70–75. URL: <https://iiste.org/Journals/index.php/JBAH/article/view/15170>.
- Wahome, M.W., Njagi, L.W., Nyaga, P.N., Mbuthia, P.G., Bebera, L.C., Bwana, M.O., 2017. Occurrence of antibodies to infectious bursal disease virus in non-vaccinated indigenous chicken, ducks and turkeys in Kenya. *International Journal of Veterinary Sciences* 6, 159–162. URL: <http://erepository.uonbi.ac.ke/handle/11295/103434>.
- Wieczorek, K., Szutkowska, B., Kierzek, E., 2020. Anti-influenza strategies based on nanoparticle applications. *Pathogens* 9. [10.3390/pathogens9121020](https://doi.org/10.3390/pathogens9121020).
- Wu, Y.N., Shieh, D.B., Yang, L.X., Sheu, H.S., Zheng, R., Thorndarson, P., Chen, D.H., Braet, F., 2018. Characterization of iron coregold shell nanoparticles for anti-cancer treatments: Chemical and structural transformations during storage and use. *Materials* 11. [10.3390/ma11122572](https://doi.org/10.3390/ma11122572).
- Yadavalli, T., Shukla, D., 2017. Role of metal and metal oxide nanoparticles as diagnostic and therapeutic tools for highly prevalent viral infections. *Nanomedicine* 13, 219–230. [10.1016/j.nano.2016.08.016](https://doi.org/10.1016/j.nano.2016.08.016).
- Zhu, L.Q., Wu, S.L., Zhang, G.P., Zhu, G.Q., 2008. The cellular receptors for infectious bursal disease virus. *African Journal of Biotechnology* 7, 4832–4835. URL: <http://www.academicjournals.org/AJB>.
- Zierenberg, K., Nieper, H., van den Berg, T.P., Ezeokoli, C.D., Voss, M., Müller, H., 2000. The VP2 variable region of african and german isolates of infectious bursal disease virus: Comparison with very virulent, "classical" virulent, and attenuated tissue culture-adapted strains. *Archives of Virology* 145, 113–125. [10.1007/s007050050009](https://doi.org/10.1007/s007050050009).